

General Disclaimer

One or more of the Following Statements may affect this Document

- This document has been reproduced from the best copy furnished by the organizational source. It is being released in the interest of making available as much information as possible.
- This document may contain data, which exceeds the sheet parameters. It was furnished in this condition by the organizational source and is the best copy available.
- This document may contain tone-on-tone or color graphs, charts and/or pictures, which have been reproduced in black and white.
- This document is paginated as submitted by the original source.
- Portions of this document are not fully legible due to the historical nature of some of the material. However, it is the best reproduction available from the original submission.

N59 7002

(NASA-CR-148599) THERMAL AND MECHANICAL
STRUCTURE OF THE UPPER MANTLE: A COMPARISON
BETWEEN CONTINENTAL AND OCEANIC MODELS
(California Univ.) 39 p HC \$4.00 CSCL 08G

N76-29787

Unclas
G3/46 49730

THERMAL AND MECHANICAL STRUCTURE OF THE
UPPER MANTLE: A COMPARISON BETWEEN
CONTINENTAL AND OCEANIC MODELS

C. Froidevaux

Laboratoire de Physique des Solides*
Université Paris-Sud
Orsay, France 91405

G. Schubert and D. A. Yuen
Department of Geophysics and Space Physics
University of California
Los Angeles, California 90024

*Laboratoire associé au CNRS



ABSTRACT

Temperature, velocity and viscosity profiles for coupled thermal and mechanical models of the upper mantle beneath continental shields and old ocean basins show that under the continents, both tectonic plates and the asthenosphere, are thicker than they are beneath the oceans. The minimum value of viscosity in the continental asthenosphere is about an order of magnitude larger than in the shear zone beneath oceans. The shear stress or drag underneath continental plates is also approximately an order of magnitude larger than the drag on oceanic plates. Effects of shear heating may account for flattening of ocean floor topography and heat flux in old ocean basins.

INTRODUCTION

Plate tectonics has stressed the importance of the concepts of lithosphere, the rigid surface layer of the Earth which is divided into a mosaic of moving plates, and of asthenosphere, a softer layer under the plates facilitating the mechanical decoupling with the lower mantle. The concept of an asthenosphere was derived long ago from the study of isostasy. On the other hand, the physical structure of the upper mantle has been discussed either on the basis of seismic velocity distributions derived from observations (Press, 1972; Knopoff, 1972; Jordan, 1975), or on the basis of purely thermal models (McKenzie, 1967; Sclater and Francheteau, 1970; Turcotte and Oxburgh, 1972). Both of these latter approaches have led to the conclusion that the physical structure is different under oceans and under continents. It is, however, difficult to make quantitative comparisons between seismological data and theoretical thermal profiles, since this involves a precise description of the petrological state of the mantle. For oceanic plates alone other geophysical data like topography have been used to test theoretical thermal models (Sorokhtin, 1973; Davis and Lister, 1974; Parsons and Sclater, 1975; Oldenburg, 1976). Convective models have not focused on the distinction between oceanic and continental regions.

Here we present models of the upper mantle wherein both the thermal and flow velocity profiles are calculated on the basis of coupled thermal and mechanical equations satisfying simple geophysical boundary conditions (Froidevaux and Schubert, 1975; Schubert et al., 1976). This is illustrated in Figure 1 which shows the oceanic model on the left, and the continental one on the right. The boundary conditions indicated in the figure, are that the temperature and horizontal velocity at the surface be T_0 and u_0 , and that the horizontal velocity at great depth be zero. In the continental case the heat flows at the surface q_0 and at great depth q_∞ are also imposed, whereas in the oceanic case, the temperature at great depth T_∞ and the vanishing of the vertical velocity at the surface are specified. The physical quantities to be calculated are also listed in the figure; they are temperature T , horizontal velocity u , shear stress τ and viscosity, and, for the oceanic case only, vertical velocity v . Except for τ , these quantities vary with depth y . In the oceanic case they all vary with horizontal distance from the ridge x , i.e. with age x/u_0 . Given a petrologic model of the mantle, seismic velocity profiles can also be computed.

All models are based on the law of deformation of olivine (Post, 1973; Kohlstedt et al., 1975)

$$\dot{\epsilon} = \frac{B_3 T^3}{T} \exp\left(-\frac{E^* + pV^*}{RT}\right) \quad (1)$$

where T is the absolute temperature, p is the pressure, $\dot{\epsilon} \equiv \frac{1}{2} du/dy$ is the strain rate, and R is the gas constant. The proportionality constant B_3 and the activation energy E^* have been measured in the laboratory, whereas the activation volume V^* has to be estimated. The justification for a model based on olivine is that this mineral is the most abundant in the mantle and it deforms more readily than other minerals in most mantle-derived peridotite samples (Boullier and Nicolas, 1973). The coupling between velocity and temperature comes about through the T -dependence of (1) and through the viscous heating term $2\tau\dot{\epsilon}$ in the temperature equation. In the continental case the temperature equation also contains a radioactive heating term Q_m and a vertical conduction term. The continental mantle is overlain by a crust divided in 2 layers. Radioactive heat generation Q_1 in the upper 8 km is a given quantity, whereas the volumetric heat production Q_2 for the 32 km thick lower crust has to be calculated to satisfy the boundary conditions. In the oceanic case the temperature equation contains both horizontal and vertical advection of heat, vertical conduction of heat and viscous dissipation. Since horizontal advection of heat is a dominant effect, radioactive heating has been neglected in this presentation. The vertical velocity in the oceanic model requires consideration of another mechanical equation, the continuity equation.

These models imply a mechanical decoupling between the surface, moving at velocity u_0 , and deeper regions. They do not fix, a priori, the depth of the shear zone nor the magnitude of τ . Since no return flow is assumed at shallow depth, the momentum equation simply states that τ is independent of y ; in the oceanic case it will however vary with x , the horizontal coordinate or age.

The system of equations just described contains no time dependence. The models should thus apply in regions where steady state might exist. We assume this to be the case for oceans and for old shields (Polyak and Smirnov, 1968). The quasi-equality of heat flow for old continental shields and old ocean basins has been considered a paradox. Our models should tell us something about this problem. They should also lead to an interesting comparison of the lithosphere-asthenosphere structures of both regions. Such comparisons will be presented in section 3, after the most striking characteristics of the models have been reviewed for continents in section 1 and for oceans in section 2. Further details and mathematical formulations are given in Froidevaux and Schubert (1975) and Schubert et al. (1976).

1. TEMPERATURE AND VELOCITY UNDER OLD CONTINENTAL SHIELDS

The values of the rheological parameters in (1) depend on the amount of volatiles, particularly water, present in the mantle (Carter and Avé Lallemant, 1970; Stocker and Ashby, 1973). It is therefore useful to test the behavior of our thermo-mechanical model when B_3 , E^* and V^* have values appropriate to wet or dry olivine. This is illustrated in Figure 2, where solutions are drawn for extreme values of V^* (11 and 30 cm³/mole) for a continental system with mantle radioactivity but without heat flow from great depth. The hatched areas in Figure 2 indicate the range of solutions for intermediate values of V^* . Other parameter values are listed in the figure caption. The temperature rises monotonically to a final value depending mainly upon V^* . This dependence reflects the contribution of shear heating to the thermal state. The velocity drops from its surface value, 5 cm/yr, to zero in a shear zone or asthenosphere beneath the rigid plate or lithosphere. The depth of the shear zone is shallow or the lithosphere is thin when the pressure dependence in (1) is strong, i.e. when V^* is large. A larger activation volume also yields a thinner asthenosphere. These characteristics are shown by the dotted bands representing the shear zones for the various solutions. The temperature and velocity profiles are relatively insensitive to whether the mantle is wet or dry. One remarkable property of all these solutions, is that the viscosity reaches

about the same minimum value of 10^{21} poise in the shear zone, or asthenosphere. Thermo-mechanical coupling leads to self-adjustment of the temperature and of the depth of the asthenosphere, so that the values of the rheological parameters do not influence the value of the viscosity minimum.

What variables in our continental models have a major influence on the viscosity value in the asthenosphere? There are two: the amount of radioactive heat sources in the mantle and the plate velocity. The effects of radiogenic heating in the mantle Q_m are seen in Figure 3 which presents continental solutions for $u_0 = 2$ cm/yr with $Q_m = 0$ HGU and $Q_m = 0.06$ HGU (1 HGU = 10^{13} cal/cm³ sec). The addition of radioactivity raises the temperature at all depths, moves the asthenosphere upward and reduces the value of the minimum viscosity by an order of magnitude. By comparing solutions in Figures 2 and 3 for $V^* = 11$ cm³/mole and $Q_m = 0.06$ HGU one finds that an increase in plate velocity from 2 to 5 cm/yr lowers the viscosity by another factor of 4. The viscosity profile for $V^* = 11$ cm³/mole, $Q_m = 0.06$ HGU and $u_0 = 5$ cm/yr is shown as the dashed curve in Figure 3. The computed shear stress τ , i.e. the drag under the continental plate, also decreases with increases in mantle radioactivity and plate velocity. For the cases in Figure 3 with $u_0 = 2$ cm/yr, the τ values are 114 bars for $Q_m = 0$ HGU and 27.2 bars for $Q_m = 0.06$ HGU; in the latter case τ drops to 17.1 bars when u_0 is increased to 5 cm/yr. This decrease of τ with u_0 is not as

strong as that found by Froidevaux and Schubert (1975) in situations where viscous heating was the dominant effect in the mantle and τu_0 was almost constant in the velocity range investigated.

Comparisons with the Earth have been attempted and the results are shown in Figure 4. Since the activation volume is not known we imposed an additional constraint on the model, namely that the geotherm is required to pass through the data points (shaded areas in Figure 4) derived from phase equilibria in kimberlite nodules from the South-African shield (Boyd, 1973; MacGregor and Basu, 1974). Only the unperturbed branch (Green and Guéguen, 1974) of this experimentally determined geotherm is used. Solutions for wet (Post, 1973) and dry (Kohlstedt and Goetze, 1974) olivine rheological parameters are obtained with $q_\infty = 0.1$ HFU, the imposed heat flow from the deep mantle. This value of q_∞ corresponds to an estimate of the adiabatic temperature gradient. The temperature solutions in Figure 4, which approximately satisfy the nodule data, are relatively insensitive to the value of the activation volume. Thus the model geotherms alone do not provide much of a constraint on the value of V^* . However, since the sheared nodules in kimberlites are thought to originate at depths of about 180 km or somewhat deeper (Boullier and Nicolas, 1973), one can use the depth of the shear zone in the model solutions as an additional constraint on acceptable models and appropriate values of V^* .

For wet olivine, a V^* between 20 and 28 cm^3/mole would give models with acceptable temperatures and shear zones starting at depths between about 225 km and 180 km, respectively. For dry olivine, no solutions could be found which simultaneously satisfied the constraints in both temperature and depth to the top of the shear zone (depth at which $u/u_0 = 0.95$). In the case of dry olivine V^* values of 16 and 20 cm^3/mole yield models with shear zones starting at depths of about 305 km and 260 km, respectively.

The viscosity minima for both the wet and dry solutions have values of about 10^{21} poise. The shear stresses for these solutions are about 80 bars, in agreement with values proposed by Goetze and Kohlstedt (1973) on the basis of dislocation studies in mantle derived peridotite nodules. The heat generation values Q_2 in the lower crust range from 0.75 to 0.8 HGU, about 40% to 35% lower than averaged values for gabbro. In these solutions, the granitic upper crustal layer had $Q_1 = 5$ HGU and $Q_m = 0.06$ HGU was specified for the mantle down to 500 km depth.

In conclusion, if a steady state regime is assumed to exist under old continental shields, our coupled thermo-mechanical model is capable of satisfactorily predicting the physical structure of the upper mantle. The finite thickness asthenosphere underlying the rigid lithosphere is a consequence of the strong T and p dependences of the mechanical constitutive equation (1). Under old continents the

depth of the asthenosphere is determined mainly by V^* , whereas its 'softness' is essentially governed by Q_m and u_o . Shear wave velocity profiles computed on the basis of solid state data for pure olivine and our model geotherms are flat. This agrees with seismological data and emphasizes that the seismological low velocity zone, which does not exist under old continental shields, is not equivalent to the shear zone or asthenosphere.

2. TEMPERATURE AND VELOCITY UNDER OLD OCEANIC BASINS

For oceanic plate models, the two-dimensional flow field u and v and temperature profile depend not only upon depth but also upon distance from the ridge as pictured in Figure 1. The boundary conditions do not include the surface heat flow, since this quantity is not well known. Instead we have imposed the temperature T_{∞} at great depth. This quantity is not known either, so that several values between 1200°C and 1600°C have been used. This boundary condition has the advantage of making a comparison with purely thermal models simple. All models in this and the remaining parts of the paper are based upon a dry olivine rheology.

The temperature profiles are dominated by heat advection, i.e. by lithospheric and asthenospheric cooling. This is particularly true for high T_{∞} values and slow plates. For a rather cool asymptotic temperature $T_{\infty} = 1200^{\circ}\text{C}$ and a high plate velocity $u_0 = 10$ cm/yr, Figure 5 shows solutions for 2 ages, 10 and 150 My. For 10 My the T profile is almost identical to the purely thermal solution calculated for the same variable thermal conductivity (dotted curve). The velocity profiles $u(y)$ and $v(y)$ are seen to depend on the value of V^* ; the shear zone is shallower when V^* is large, as was found in the continental models. In Figure 5 the hatched areas indicate again the range of solutions for intermediate

values of V^* . The viscosity minimum is less than 10^{21} poise, for $T_\infty = 1600^\circ\text{C}$ it drops below 10^{20} poise. The vertical velocity v increases from zero to an asymptotic value in the region where the horizontal velocity drops to zero, i.e. in the asthenosphere. The finite value of v at great depth provides a mass flow necessary for the accretion of the thickening lithosphere. For an age of 150 My Figure 5 shows that the temperature profile departs strongly from the purely thermal cooling solution (dotted curve). This is due to shear heating, an effect which is stronger for larger values of V^* . The viscosity in the asthenosphere is somewhat higher beneath old oceans. At 150 My the upward velocities are an order of magnitude smaller than at 10 My.

Shear heating generates marked departures from a simple $\sqrt{\text{age}}$ dependence for derived quantities like lithosphere thickness, topography and heat flow. This is illustrated in Figure 6 for the first two of these geophysical quantities. The lithosphere thickness, defined as the depth at which u falls to 95% of the surface value u_0 , increases with age, but not as fast as a $\sqrt{\text{age}}$ law which would yield a straight line on this plot. As mentioned earlier the thickness is smaller for larger V^* values. For each value of V^* the upper and lower curves correspond to u_0 values of 10 cm/yr and 2 cm/yr, respectively. Shear heating is stronger for larger u_0 values; consequently the lithospheric plate is somewhat thinner. The

topography of the ocean floor represented in Figure 6 by the water-depth also departs from a $\sqrt{\text{age}}$ law indicated by the dashed straight line. The departure is very pronounced for $V^* = 30 \text{ cm}^3/\text{mole}$. The experimental points redrawn from Parsons and Sclater (1975) could be fitted for a V^* value just above $11 \text{ cm}^3/\text{mole}$. This topography model reflects the gradual cooling of the lithosphere and asthenosphere; it was computed for a thermal expansion coefficient $\alpha = 4 \times 10^{-5} \text{ K}^{-1}$. No data is available for the lithospheric thickness as defined here. The depth of origin of sheared peridotite nodules might in the future give some constraints. For now we can only say that the depth to the seismic low velocity zone inferred from surface and body wave data increases monotonically up to ages as old as 150 My (Leeds, 1975; Sipkin and Jordan, 1976). The ocean floor heat flow data, on the other hand are too controversial to warrant a detailed comparison. Our models of q_0 for $T_\infty = 1200^\circ\text{C}$ also show a certain amount of flattening, i.e., a departure from an $(\text{age})^{-1/2}$ proportionality for heat flow. Viscous dissipation provides additional heat to the old ocean floor. Stress values increase by factors of 2 to 5 for the cases shown above as age increases. They are less than 80 bars for solutions based on the rheology of dry olivine. For a wet olivine rheology, stresses and shear heating effects are reduced by factors of 2 to 3. They are also reduced for larger T_∞ values, $T_\infty = 1200^\circ\text{C}$ being the value applicable to

Figures 5 and 6.

In summary, for young ages thermo-mechanical coupling beneath oceans is negligible and the T profiles are close to the solutions for simple boundary layer cooling. Note however that although the isotherms for such purely thermal solutions are parabolic, they would not yield a parabolic lithosphere because of the pressure dependence of the viscosity implied by equation (1). A second point to emphasize is that departures from $\sqrt{\text{age}}$ laws at old ages are a result of distortion of the geotherms by shear heating. This explanation of known geophysical behavior (see topography) is more satisfactory than that based on the ad hoc representation of the lithosphere by a slab of constant thickness (Parsons and Sclater, 1975). The stage is now set for a comparison of continents and oceans.

3. A DIRECT COMPARISON OF CONTINENTAL AND OCEANIC MODELS BASED ON A DRY OLIVINE RHEOLOGY.

So far we have shown that the one-dimensional flow field under old continental shields, as well as the two-dimensional flow field under oceanic plates, and their associated temperature fields can be modelled on the basis of simple geophysical boundary conditions and physical properties corresponding to the thermal conductivity and rheology of olivine as measured in the laboratory.

A comparison of the situations under old continents and under old oceanic basins can be undertaken. This requires an appropriate matching of boundary conditions. We shall proceed in the following way. First we take $T_0 = 0^\circ\text{C}$, $q_0 = 1.05$ HFU (1HFU = 10^{-6} cal/cm² sec) for continental shields and compute solutions corresponding to $q_\infty = 0$ HFU. This yields a computed temperature T_∞ at great depth under old continents. We then compute oceanic solutions for the same T_0 and T_∞ values, and of course for the same surface velocity u_0 . All this is carried out under the assumption that mantle rheological properties are identical to those of dry olivine and are the same under ocean basins and under continental shields. Since the activation volume V^* has not been measured in the laboratory, we present solutions for $11 \leq V^* \leq 30$ cm³/mole.

In the oceanic models, where horizontal and vertical ad-

vection of heat dominates, we shall neglect the thin basaltic crust as well as mantle radioactivity. However the continental models not only include a radioactive crust with $Q_1 = 5$ HGU and a lower crust with a Q_2 value which has to be computed, but also a radioactive upper mantle with $Q_m = 0.06$ HGU, a reasonable average value. We realize that the true value of Q_m is not well determined; for example Sorokhtin (1974) has argued that its value could be zero. In any case, although the specific comparison discussed here is based on a continental model with nonzero Q_m we can use the results of Figure 3 to infer the effect of a smaller or zero value of Q_m beneath continents. Shear heating is, of course, included in both oceanic and continental models.

Figure 7 gives continental and oceanic solutions for $u_o = 2$ cm/yr. For $V^* = 11$ cm³/mole and 30 cm³/mole, the continental solutions have $T_\infty = 1392$ °C, $Q_2 = 1.04$ HGU and $T_\infty = 1665$ °C, $Q_2 = 0.59$ HGU, respectively. The corresponding oceanic geotherms for an age of 150 My have surface heat flow values of 0.82 and 0.98 HGU, respectively. Both the surface heat flows in the oceanic cases and the lower continental crustal radioactivity have reasonable values when compared with geophysical and geochemical data.

What are the most striking points emerging from a comparison of the solutions in Figure 7? Firstly, we see that the oceanic geotherm is everywhere higher than the corres-

ponding continental one and thus has a much steeper gradient at shallow depths. This is basically due to the existence of a thick radioactive crust for the continents. As a consequence the lithospheric thickness is larger under continental shields than under old oceanic basins. This is pictured by the position of the top boundary of the dotted bands representing the depth range of the asthenosphere (defined by $0.05 \leq u/u_0 \leq 0.95$). The asthenosphere beneath continents is thicker than that under oceans. The value of the viscosity minimum in the continental asthenosphere is essentially an order of magnitude larger than that in the oceanic shear zone. Similarly the drag under the continental plate is about an order of magnitude larger than that beneath the oceanic plate. The drag is given by the computed value of shear stress τ which is 4.9 and 27.2 bars for the oceanic and continental cases, respectively, when $V^* = 11 \text{ cm}^3/\text{mole}$; corresponding τ values for $V^* = 30 \text{ cm}^3/\text{mole}$ are 10.7 and 124 bars. These results compare favorably with those of Forsyth and Uyeda (1975) and Solomon et al. (1975) who suggest a larger drag under continental plates on the basis of analyses of plate motions.

To discuss the relative importance of the various heat sources beneath the oceans and continents we have constructed Table 1 from the solutions of Figure 7. In order to make vertical heat advection into the oceanic lithosphere negligible

we now define the base of the oceanic lithosphere as the depth for which $u = 0.995 u_0$. For consistency we apply the same definition of lithospheric base to the continental case, even though there is no advection in the continental models. Given this definition we can read the entries in Table 1 for lithospheric thickness and sublithospheric temperature directly from Figure 7. The heat flux into the base of the lithosphere, q_L , is computed as the product of thermal conductivity and temperature gradient at the appropriate depth from the detailed solutions. The difference between surface heat flow q_0 and q_L is either the contribution of lithosphere radioactivity to q_0 in the continental case or the contribution of horizontal advection to q_0 in the oceanic case.

Table 1 shows that a substantial fraction (1/3 to 2/3) of the surface heat flow in the old ocean floor comes from the cooling of the lithosphere as it thickens and moves away from the ridge. The remainder of the surface heat flow derives from asthenospheric cooling, vertical advection, and viscous dissipation τu_0 . The source of the continental surface heat flux is radiogenic heating in the crust (55 to 70%) and in the mantle (26%), and viscous dissipation (19 to 4%).

Sclater and Francheteau's (1970) purely conductive model of the oceanic lithosphere does not include advection of heat. Our results show that this is still important even for an age of 150 My and must be included when the "equality"

of heat flow between continental shields and oceanic basins is discussed. One should notice finally that the sub-asthenospheric temperature is considerably higher (200-400°C) than the temperature just under the plates. In the literature these 2 quantities are often indiscriminately equated, just as the constant thickness slab introduced by McKenzie (1967) for mathematical convenience is often presented as the lithosphere.

CONCLUDING REMARKS

This paper has shown that it is possible to construct satisfactory models of the upper mantle beneath both continents and oceans. Under the oceans, the plates are found to be thinner, the asthenosphere softer and hence the drag smaller than under the continents. The comparison of continental and oceanic models with each other and with the real earth would be improved by including radioactivity under the oceans and by accounting for a nonzero heat flux from great depth. Further improvement would require additional data on possible lateral heterogeneities in the distribution of radioactive heat sources and in the rheological properties of the mantle.

ACKNOWLEDGMENT

This work was partly supported by the Earth Sciences Section, National Science Foundation, NSF Grant GA 40749 and by the National Aeronautics and Space Administration, NSG 7002.

REFERENCES

- Boyd, F. R., A pyroxene geotherm, Geochim. et Cosmochim. Acta, 37, 2533-2546, 1973.
- Boullier, A. M., and A. Nicolas, Texture and fabric of peridotite nodules from kimberlites, in Lesotho Kimberlites, edited by P. H. Nixon, pp. 57-66, Lesotho National Dev. Corp., Maseru, 1973.
- Carter, N. L., and H. G. Avé Lallemant, High temperature flow of dunite and peridotite, Geol. Soc. of America Bulletin, 81, 2181-2202, 1970.
- Davis, E. E. and C. R. B. Lister, Fundamentals of ridge crest topography, Earth Planet. Sci. Lett., 21, 405-413, 1974.
- Forsyth, D. and S. Uyeda, On the relative importance of the driving forces of plate motion, Geophys. J. Roy. Astron. Soc., 43, 163-200, 1975.
- Froidevaux, C. and G. Schubert, Plate motion and structure of the continental asthenosphere: A realistic model of the upper mantle, J. Geophys. Res., 80, 2553-2564, 1975.
- Goetze, C., and D. L. Kohlstedt, Laboratory study of dislocation climb and diffusion in olivine, J. Geophys. Res., 78, 5961-5971, 1973.
- Green, H. W. II., and Y. Gueguen, Origin of kimberlite pipes by diapiric upwelling in the upper mantle, Nature, 249, 617-620, 1974.
- Jordan, T. H., The continental tectosphere, Rev. Geophys. Space Phys., 13, 1-12, 1975.

- Knopoff, L., Observation and inversion of surface wave dispersion, Tectonophysics, 13, 497-519, 1972.
- Kohlstedt, D. L. and C. Goetze, Low Stress, High Temperature Creep in Olivine Single Crystals, J. Geophys. Res., 79, 2045-2051, 1974.
- Kohlstedt, D. L., C. Goetze and W. B. Durham, Experimental deformation of single crystal olivine with application to flow in the mantle, Proc. 1974 NATO Conf. on Petrophysics, Newcastle-upon Tyne, in press, 1975.
- Leeds, A. R., Lithospheric thickness in the western Pacific, Phys. Earth Planet. Interiors, 11, 61-64, 1975.
- MacGregor, I. D., and A. R. Basu, Thermal structure of the lithosphere; a petrologic contribution, Science, 185, 1007-1011, 1974.
- McKenzie, D. P., Some remarks on heat flow and gravity anomalies, J. Geophys. Res., 72, 6261-6273, 1967.
- Oldenburg, D. W., A Physical Model for the Creation of the Lithosphere, in press, Geophys. J. Roy. Astr. Soc., 1976.
- Parsons, B. and J. G. Sclater, An analysis of the variation of ocean floor heat flow and bathymetry with age, submitted to Geophys. J. Roy. Astron. Soc., 1975.
- Polyak, B. G. and Y. B. Smirnov, Relationship between heat flow and the tectonics of continents, Geotectonics, 4, 205-213, 1968.

Post, R. L., The flow laws of Mount Burnett dunite, Ph.D. thesis, Univ. of Calif., Los Angeles, 1973.

Press, F., The earth's interior as inferred from a family of models, in The Nature of the Solid Earth, edited by E. C. Robertson, pp. 147-171, McGraw-Hill, New York, 1972.

Schatz, J. F. and G. Simmons, Thermal conductivity of earth materials at high temperatures, J. Geophys. Res., 77, 6966-6983, 1972.

Schubert, G., C. Froidevaux and D. A. Yuen, Oceanic lithosphere and asthenosphere: thermal and mechanical structure, submitted to J. Geophys. Res., 1976.

Sclater, J. G. and J. Francheteau, The implication of terrestrial heat flow observations on current tectonic and geochemical models of the crust and upper mantle of the earth, Geophys. J. Roy. Astro. Soc., 20, 509-537, 1970.

Sclater, J. G., New perspectives in terrestrial heat flow, Tectonophysics, 13, 257-291, 1972.

Sipkin, S. A. and T. H. Jordan, Lateral heterogeneity of the upper mantle determined from travel times of multiple ScS, submitted to J. Geophys. Res., 1976.

Solomon, S. C., N. H. Sleep and R. M. Richardson, On the forces driving plate tectonics: Inferences from absolute plate velocities and intraplate stress, Geophys. J. Roy. Astr. Soc., 42, 769-803, 1975.

Sorokhtin, O. G., Global Evolution of the Earth (in Russian),
"Science" edition, Moscow, 1974.

Stocker, R. L., and M. F. Ashby, on the rheology of the upper
mantle, Reviews of Geophys. and Space Phys., 11, 391-426,
1973.

Turcotte, D. L. and E. R. Oxburgh, Mantle convection and
the new global tectonics, Ann. Rev. Fluid Mech., 4,
33-68, 1972.

	$V^* = 11 \text{ cm}^3/\text{mole}$		$V^* = 20 \text{ cm}^3/\text{mole}$	
	Ocean (150 My)	Continent	Ocean (150 My)	Continent
Lithospheric thickness L (km)	140	245	95	185
Sublithospheric temperature T_L ($^{\circ}\text{C}$)	1225	1185	1190	1260
Temperature below the asthenosphere T_{∞} ($^{\circ}\text{C}$)	1392	1392	1665	1665
Heat Flux into the lithosphere q_L (HFU)	0.28	0.19	0.63	0.37
Contribution of lithosphere radioactivity to q_O (HFU)	-	0.86	-	0.68
Contribution of advection to q_O (HFU)	0.54	-	0.35	-
Surface heat flow q_O (HFU)	0.82	1.05	0.98	1.05
Contribution of shear heating τu_O to q_L (HFU)	0.0074	0.041	0.016	0.19

Table 1. Comparison of thermal states under old oceans and continental shields.

FIGURE CAPTIONS

Figure 1. Oceanic (left) and continental (right) models. The boundary between lithosphere and asthenosphere appears to be sharp for artistic reasons only; its depth is not a specified parameter. For the oceanic case the temperature T_0 , horizontal and vertical velocities u_0 and v_0 at the surface, as well as the temperature T_∞ and the zero horizontal velocity $u = 0$ at great depth are given as boundary conditions. For the continental case the boundary conditions are the temperature T_0 , the velocity u_0 and the heat flow q_0 at the surface, as well as the heat flow q_∞ and zero velocity $u = 0$ at great depth. The continental mantle has a volumetric radiogenic heat-source Q_m . It is overlain by a crust with thermal conductivity k_c . The crust has an 8 km upper layer with radiogenic heat sources Q_1 and a 32 km lower layer with unspecified radiogenic heat sources Q_2 . The quantities listed on the right hand side of both the oceanic and continental diagrams are those to be computed.

Figure 2. Temperature and velocity profiles for a wet and a dry olivine continental mantle containing radioactive heat sources. The parameter values for the wet case are $B_3 = 5.41 \times 10^{-15} \frac{\text{cm}^3 \text{sec}^5 \text{K}}{\text{gm}^3}$, $E^* = 95$ kilocal/mole (Post, 1973), and for the dry case $B_3 = 6.45 \times 10^{-13} \frac{\text{cm}^3 \text{sec}^5 \text{K}}{\text{gm}^3}$, $E^* = 125$ kilocal/mole (Kohlstedt and Goetze, 1974). The activation volume V^* was 11 or 30 cm^3/mole and the corresponding solutions are labelled accordingly. The hatched area indicates the range of solutions for intermediate values of V^* . In all of these figures, the mantle thermal conductivity model $k_m(T, z)$ of Schatz and Simmons (1972) is used. The continental crust has a top layer of 8 km with $Q_1 = 5$ HGU and a bottom layer of 32 km with the computed Q_2 value quoted in the text. The mantle radioactivity content $Q_m = 0.05$ HGU is specified down to 500 km depth. Boundary conditions are $T_0 = 0^\circ \text{C}$, $q_0 = 1.05$ HFU, $u_0 = 5$ cm/yr, $q_\infty = 0$ HFU. The computed shear stress τ is 9.3 bars ($V^* = 11 \text{ cm}^3/\text{mole}$) or 50.9 bars ($V^* = 30 \text{ cm}^3/\text{mole}$) for the wet case, and 17.1 bars ($V^* = 11 \text{ cm}^3/\text{mole}$) or 63.2 bars ($V^* = 30 \text{ cm}^3/\text{mole}$) for the dry case. The dotted bands indicate the depth range of the asthenosphere for a particular value of V^* in cm^3/mole .

The asthenosphere is defined as the depth range between $u = 0.95 u_0$ and $u = 0.05 u_0$.

Figure 3. Temperature, velocity, and viscosity profiles for a dry olivine, continental mantle. $Q_m = 0.0$ HGU or 0.06 HGU, $V^* = 11 \text{ cm}^3 \text{ mole}^{-1}$, $u_0 = 2 \text{ cm yr}^{-1}$, and $q_\infty = 0.0$ HFU. For the models with mantle radioactivity, the heat sources extend down to 500 km depth. The computed shear stresses are 27.2 bars ($Q_m = 0.06$ HGU) and 114 bars ($Q_m = 0.0$ HGU). The dashed curve is the viscosity profile for $V^* = 11 \text{ cm}^3/\text{mole}$, $Q_m = 0.06$ HGU and $u_0 = 5 \text{ cm/yr}$ ($\tau = 17.1$ bars).

Figure 4. 'Realistic' models of the upper mantle beneath continental shields. The shaded region delineates the approximate range of the pyroxene geotherms (MacGregor and Basu, 1974). Computed models of the thermal and mechanical structures are shown for a range of activation volumes for wet and dry olivine. Geotherms satisfying the paleotemperatures are relatively insensitive to the value of activation volume. An additional mechanical constraint based on the interpretation of sheared nodules (Boullier and Nicolas, 1973) is imposed on the depth of the top of the shear zone. For

wet olivine and $q_{\infty} = 0.1$ HFU, the activation volumes for the solutions which best satisfy both the thermal and mechanical constraints lie between 20 and 28 $\text{cm}^3 \text{mole}^{-1}$. For dry olivine acceptable solutions could not be found. The computed shear stresses are 88.8 bars ($V^* = 28 \text{ cm}^3/\text{mole}$), 71.9 bars ($V^* = 20 \text{ cm}^3/\text{mole}$), 62.5 bars ($V^* = 6 \text{ cm}^3/\text{mole}$) for wet olivine, and 88.1 bars ($V^* = 20 \text{ cm}^3/\text{mole}$) and 62.4 bars ($V^* = 4 \text{ cm}^3/\text{mole}$) for dry olivine.

Figure 5. Temperature, viscosity, horizontal and vertical velocity fields of an oceanic lithosphere and asthenosphere model for a dry olivine rheology. $T_{\infty} = 1200^{\circ}\text{C}$ and $u_0 = 10 \text{ cm yr}^{-1}$. Solutions are shown for two extreme values of V^* , 11 and 30 $\text{cm}^3 \text{mole}^{-1}$, and for two ages, 10 and 150 My. They are indicated in the figure by the numbers adjacent to the curves. For an age of 10 My, temperature profiles are insensitive, at the accuracy of our graph, to the value of V^* . This is not so for the velocity curves. The shaded area between two such curves represents the range of solutions for intermediate values of V^* . For an age of 150 My the temperature profiles depend on V^* . The upper curve is for

$V^* = 30 \text{ cm}^3 \text{ mole}^{-1}$ and the lower one is for $V^* = 11 \text{ cm}^3 \text{ mole}^{-1}$. The dotted curves denote the temperature profiles for simple boundary layer cooling with variable thermal conductivity. The conduction solution for 10 My is similar to the $V^* = 11 \text{ cm}^3 \text{ mole}^{-1}$ and $V^* = 30 \text{ cm}^3 \text{ mole}^{-1}$ curves. The stresses developed in these oceanic models are 11.8 bars ($V^* = 11 \text{ cm}^3/\text{mole}$), 34.0 bars ($V^* = 30 \text{ cm}^3/\text{mole}$) for 10 My and 25.8 bars ($V^* = 11 \text{ cm}^3/\text{mole}$), 75.5 bars ($V^* = 30 \text{ cm}^3/\text{mole}$) for 150 My.

Figure 6. Bathymetry of the ocean floor and lithospheric thickness (depth at which $u/u_0 = 0.95$) as a function of $(\text{age})^{1/2}$ for a dry olivine rheology with $T_\infty = 1200^\circ\text{C}$, and $V^* = 11$ and $30 \text{ cm}^3 \text{ mole}^{-1}$. For the depth of water plot, $u_0 = 10 \text{ cm yr}^{-1}$ and $\alpha = 4 \times 10^{-5} \text{ K}^{-1}$. The shaded region represents the bathymetry solutions for intermediate values of V^* . The dashed lines are the ocean floor depths for simple boundary layer cooling. The data points are taken from Parsons and Sclater (1975). For the thickness of the lithosphere curves, the value of u_0 distinguishes the solid curves with the same value of V^* ; the thicker lithosphere is for $u_0 = 2 \text{ cm yr}^{-1}$, the thinner

one is for $u_o = 10 \text{ cm yr}^{-1}$.

Figure 7. A comparison of the thermal and mechanical structures between old oceanic basins (150 My) and continental shields. Dry olivine rheology, $u_o = 2 \text{ cm yr}^{-1}$, $q_\infty = 0.0 \text{ HFU}$ and equal asymptotic temperatures, T_∞ , are required for both tectonic models. $Q_m = 0.06 \text{ HGU}$ is specified for the continental mantles down to 500 km depth. The effect of an increase in V^* is greater on continental models, which decouple at a greater depth than the oceanic ones. The viscosity minima for the oceanic cases are an order of magnitude lower than the continental values. The stresses in the continental cases (124.0 bars, $V^* = 30 \text{ cm}^3 \text{ mole}^{-1}$; 27.2 bars, $V^* = 11 \text{ cm}^3 \text{ mole}^{-1}$) are an order of magnitude greater than those found for the oceanic solutions (10.7 bars, $V^* = 30 \text{ cm}^3 \text{ mole}^{-1}$; 4.9 bars, $V^* = 11 \text{ cm}^3 \text{ mole}^{-1}$).

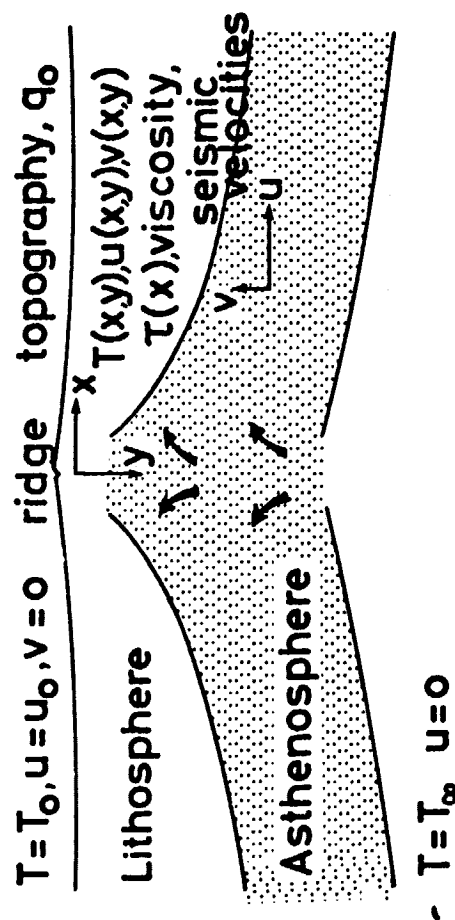
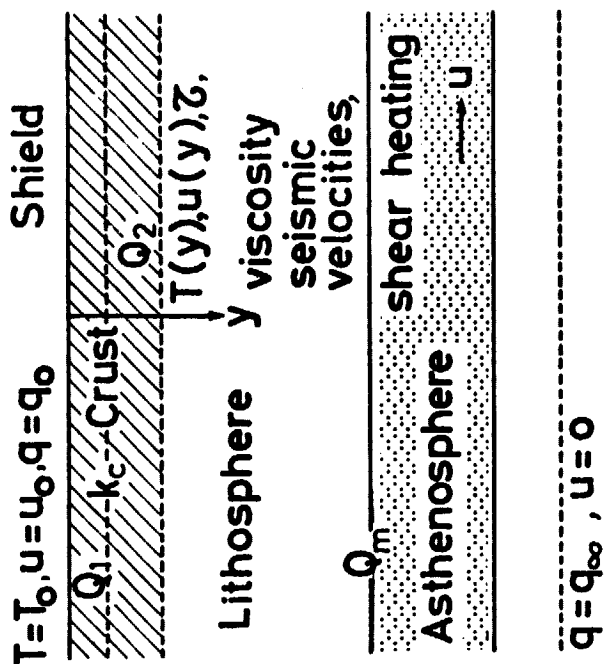


Fig.
1

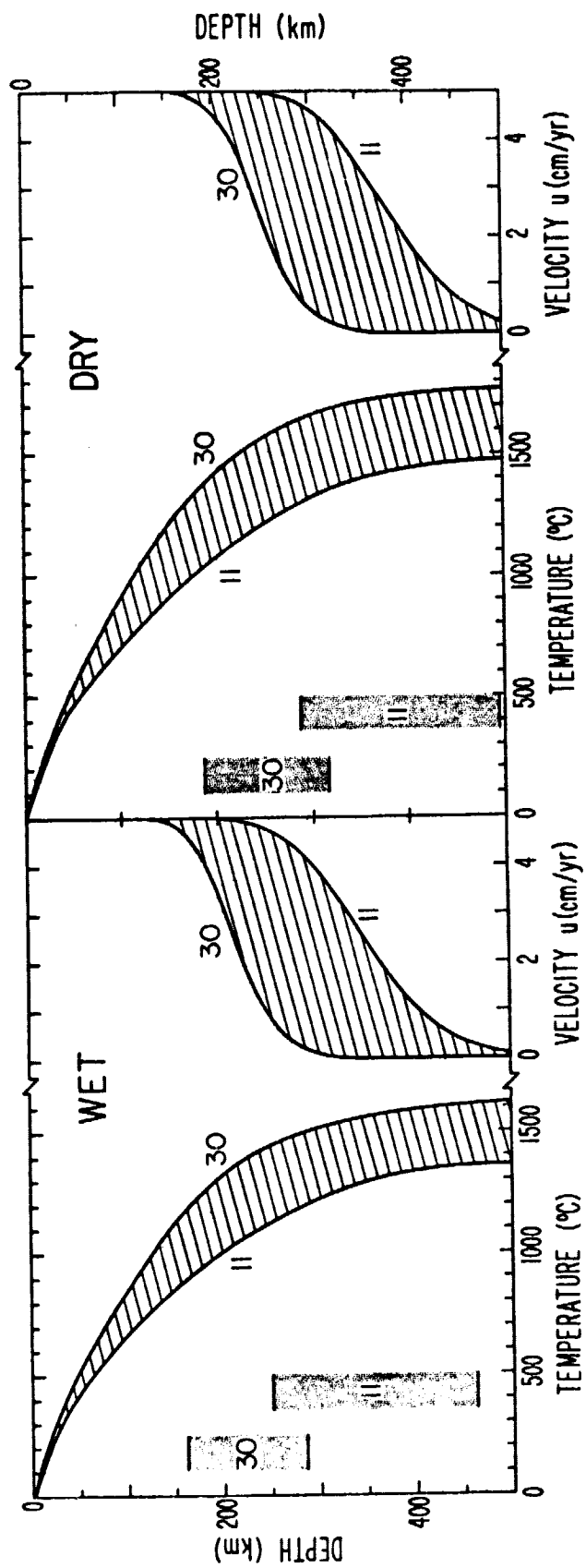


Fig.
2

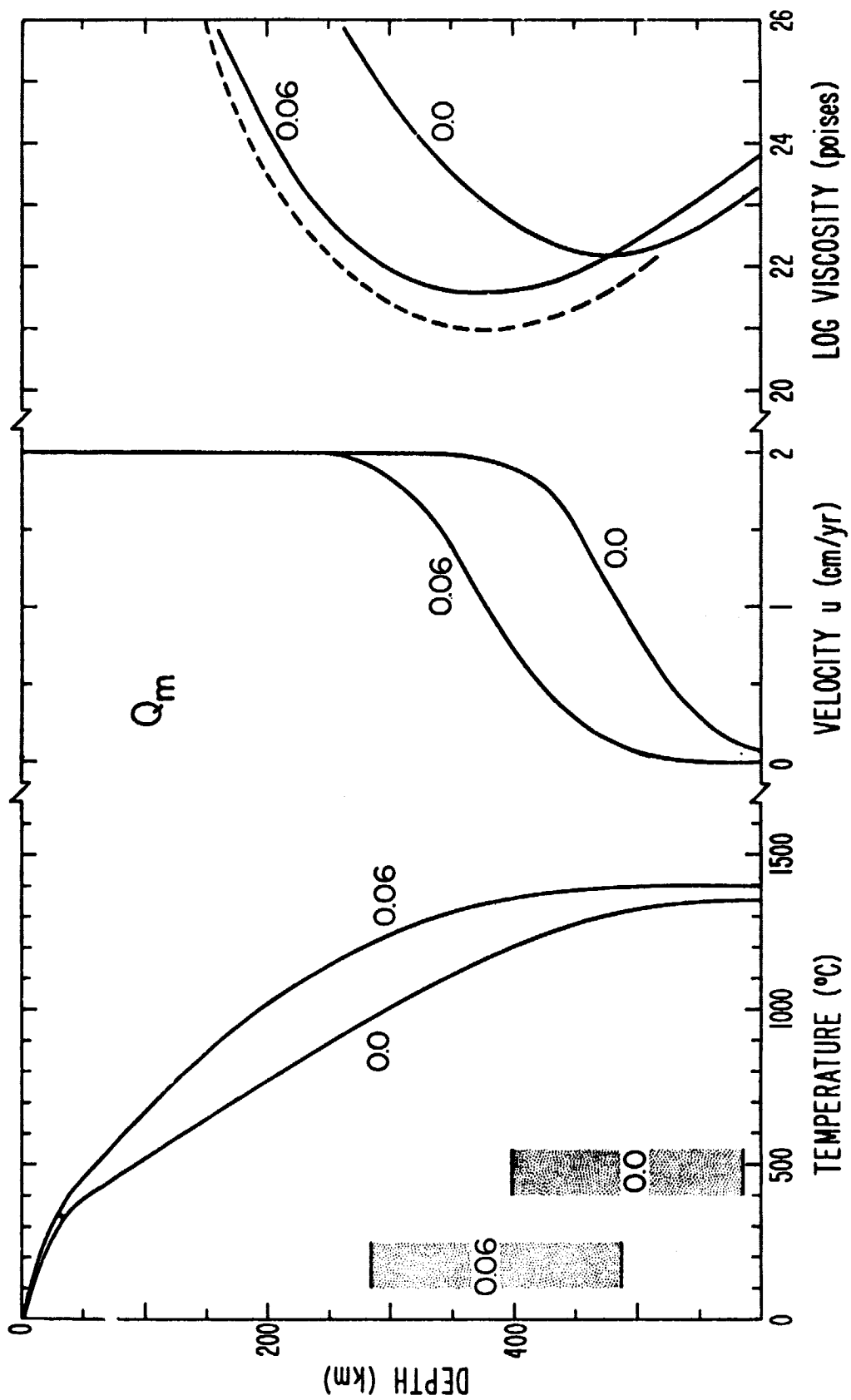


Fig.
3

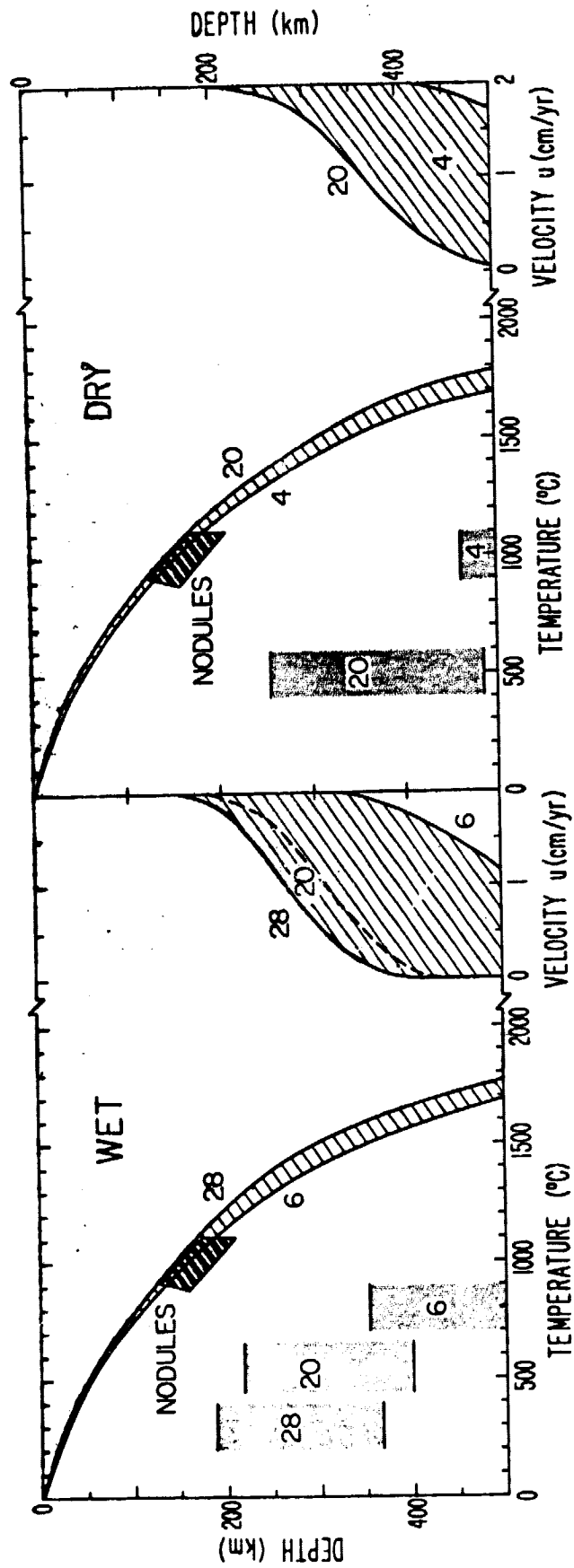


Fig.
4

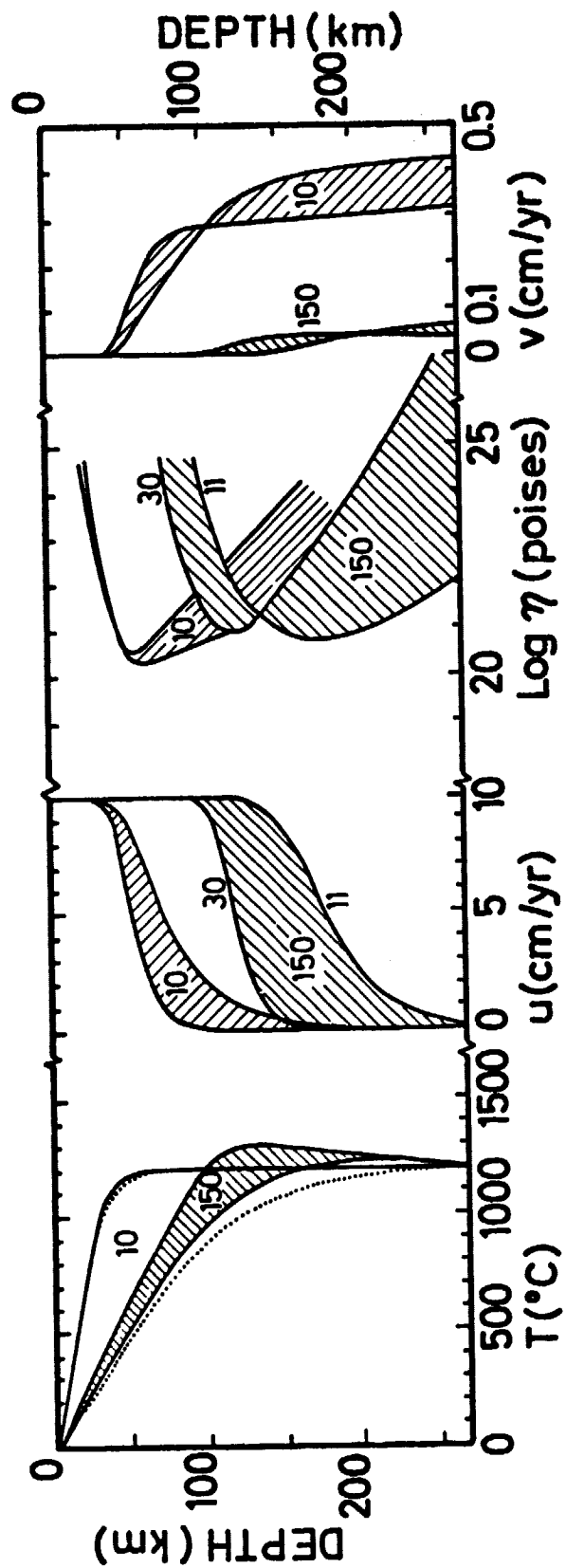


Fig.
5

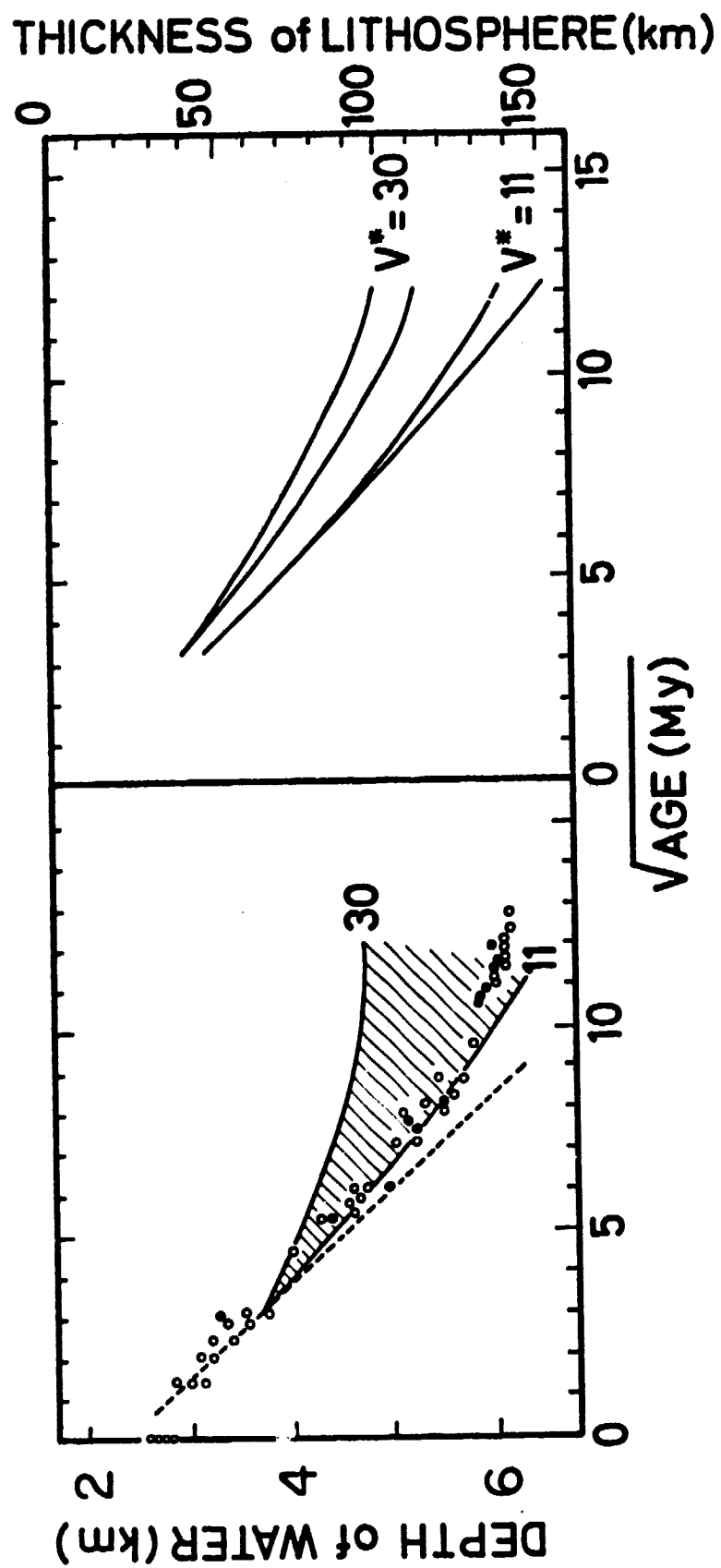


Fig.
6

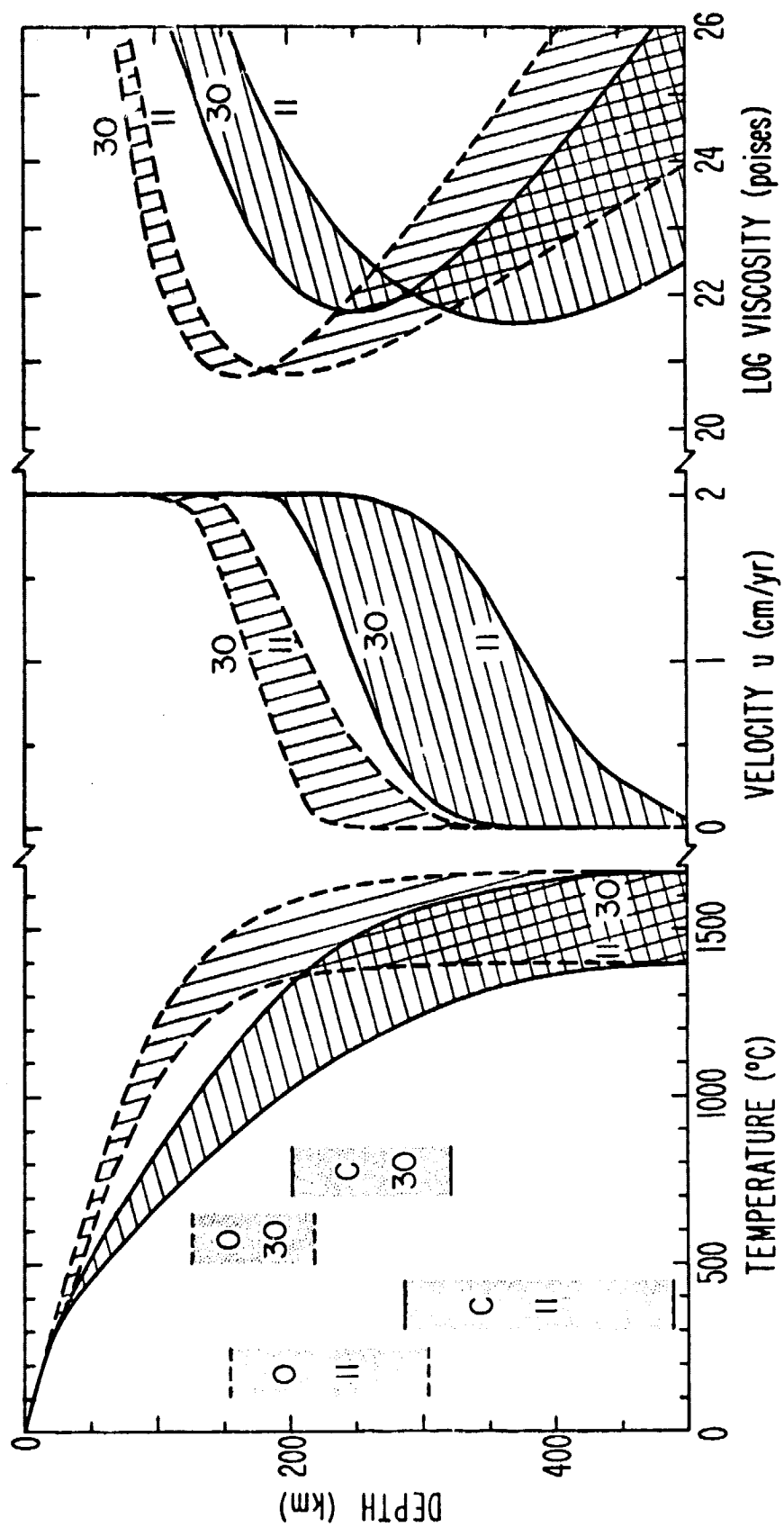


Fig.
7